DOI: 10.13009/EUCASS2017-411

Experimental validation of Unmanned Aerial Vehicles to tune PID controllers in open source autopilots

Pedro L. Jimenez, Jorge A. Silva** and Juan S. Hernandez****
**Associate Professor*
Universidad de San Buenaventura, Cr 8H N° 172 - 20 Bogota – Colombia
***Research Assistant*
Universidad de San Buenaventura, Cr 8H N° 172 - 20 Bogota – Colombia
****Research Assistant*
Universidad de San Buenaventura, Cr 8H N° 172 - 20 Bogota – Colombia

Abstract
This paper presents an experimental validation of open source and low cost autopilots for short range and fixed wing Unmanned Aerial Vehicles in order to determine a standard tune method for PID controllers applied for model airplanes using Extended Kalman Filter (EKF) and total energy control system (TECS) for attitude, speed and height tuning. The first step is to analyze the data obtained in an experimental flights and hardware in the loop (HIL) simulation interface, then, telemetry data is compared with the model airplane flight dynamics as a validation of the automatic flight control. Finally, automatic tune for PID controllers is implemented to establish new methods in future developments in Unmanned Aerial Vehicles.

1. Introduction

Present-day unmanned aircraft systems (UAS) are playing an important role in daily life; these systems perform functions in aerial photography, surveillance, reconnaissance, search and rescue, atmospheric data acquisition, among others. Therefore, to perform a specific mission in efficient and precise way, systems must be able to adjust PID controllers through algorithms as EKF (Extended Kalman Filter) and TECS (Total Energy Control System), which allows determine aircraft attitude and altitude, longitudinal control and velocity to adjust through auto-tune controllers. This paper is focused on a validation of standard methods to adjust the PID controllers present in SIG KADET model airplane, shown in figure 1. This is a fixed wing aircraft with a Pixhawk open source autopilot and Arduplane flight controller version 3.3.

Extended Kalman Filter (EKF) is an adaptation of the Kalman Filter (KF) to accommodate nonlinear systems. The EKF is a basic tool for solving estimation problems. This is used in many applications including target tracking, mobile robot localization and mapping [1] [2]. The EKF is frequently used in nonlinear estimation problems, especially attitude estimation problems of rigid bodies like Unmanned Aerial Vehicles (UAV). This tool returns quaternion approximations based on inputs of Inertial Navigation System INS, as shown in figure 2, it means that EKF is an algorithm used to estimate vehicle position, velocity and angular orientation based on gyroscopes, accelerometer, magnetometer (compass), Ground Positioning System (GPS), airspeed and barometric pressure measurements. This makes the vehicle less susceptible to faults that affect a single sensor. EKF also enables measurements from optional sensors such as optical flow and laser range finders to be used to assist navigation. An EKF is used to fuse together the sensor measurements for attitude estimation. This can recursively estimate the system states from system measurements corrupted with Gaussian noises, since both gyroscope and accelerometer sensors have Gaussian noises [3]. The advantage of the EKF over the simpler complementary filter algorithms is that by fusing all available measurements it is better to reject measurements with significant errors so that the vehicle becomes less susceptible to faults that affect a single sensor, in consequence, the use of this filter allows the system to be more reliable. Another feature of the EKF algorithm is that it is able to estimate offsets in the vehicles compass readings and also estimate the earth's magnetic field. This makes it less sensitive to compass calibration errors than current complementary filter algorithms [4]. The standard EKF exist of two main steps. First step can be called the prediction of the estimated mean of the state of the system, and uses the system dynamic equations. Also the covariance of the estimate is predicted. Second step is the measurement update [5]. Open source controller as

DOI: 10.13009/EUCASS2017-411

ArduPilot 3.3 use the EKF as primary attitude and position estimation source. Flight controller has two IMUs (Inertial Measurement Units) available that will run in parallel, each using a different IMU. The availability of faster processors such as Pixhawk have enabled more advanced mathematical algorithms to be implemented to estimate the orientation, velocity and position of the UAV.

Figure 1: SIG Kadet Senior Model Airplane UAV

Figure 2: Control system and sensors used in Kadet Senior UAV

On the other hand, another algorithm that is important to adjust PID controllers is TECS (Total Energy Control System), it is a new control strategy that was described for longitudinal flight path and speed control, in others words, is a way to address the shortcomings of SISO (Single input Single Output) flight controllers. It was first presented by A. A. Lambregts in 1983 [6] [7]. NASA sponsored Langley's research for the development of improved concepts. As a result, creation of a new architecture based on two subsystems, Flight Management Computer (FMC) and Flight Control Computer (FCC) [8] [9]. TECS was chosen for its ability to decouple altitude and speed responses, without the need to employ a more accurate model of the aircraft. For maneuvers such as landing, this decoupling is important because the aircraft in the last phase of the landing requires the ability to control the longitudinal position without minimal influence on altitude [10]. TECS uses a MIMO (Multiple Inputs Multiple Outputs) control algorithm to provide operational and performance strength in the most complete way in any of the operational modes and flight conditions. It is based on the consideration of energy management, and the result is an energy-efficient operation structure that solves most problems concerning autopilots and auto-throttle based on desired velocity and elevator deflection, important task to perform activities such as aerial photography and atmospheric data acquisition [13]. By this reason, aircraft response in altitude and speed are coupled, an increase in thrust will increase both airspeed and altitude, while a nose-up elevator command will result in increasing altitude and decreasing speed. The control responses for elevator and thrust inputs are roughly orthogonal [11]. TECS refers to a new control algorithm that manages the demand for pitch angle and regulates the control of height and speed of the aircraft. The physics that incorporates the operation of the TECS is simple, but it is necessary to know two types of mechanical energy, the gravitational potential energy (Ep) and kinetic energy (Ek), mass (m), gravity (g), height (h) and aircraft velocity (v), the most important parameters for this algorithm shown in equation 1 and 2.

$$E_P = m\,g\,h \tag{1}$$

$$E_K = \frac{1}{2}\,m\,v^2 \tag{2}$$

In addition, gravitational potential energy is the energy stored in an object due to its height and it is proportional to the height of the object and kinetic energy is the energy stored in an object due to its velocity and is proportional to the velocity squared. The aircraft total energy is the sum of the gravitational potential energy and the kinetic energy.

DOI: 10.13009/EUCASS2017-411

Total energy is continuously reduced due to the drag force acting on the aircraft, thus the height and speed are maintained only by the thrust force through the motor. TECS calculates the total energy required based on the demanded speed and height and adjusts the throttle to maintain total energy at the demanded value [12]. Besides, TECS algorithm is used to ensure a correct balance between gravitational potential energy and kinetic energy by adjusting the required pitch angle (θ). Then, lowering the nose (pitch down) energy is transferred from gravitational potential to kinetic energy or vice-versa [12]. The TECS principle is based on the idea that an elevator deflection will not have a very significant influence on the total energy (kinetic + potential) of the airplane; however, propulsion system does influence the total energy. Lift and side force (sideslip) are by definition perpendicular to the velocity vector, therefore, there is not contribution to energy, rotational kinetic energy is neglected [5]. Hence, motor is used to control the energy state of the aircraft. Total energy of the aircraft can be expressed as:

$$E_T = \frac{1}{2}mV^2 + mg(h - h_o) \quad \textbf{(3)}$$

In addition to EKF and TECS, auto-tune PID is introduced to have a well-calibrated airplane. First, a good set of roll, pitch and yaw tuning parameters are crucial for stable and precise flight. This step is achieved with trial and error tests. Manual flight adjustment is developed during this stage. Then, auto-tune mode is used in the flight controller as a flight mode that flies the airplane with assisted stabilized movements. Simple transfer functions are implemented, but changes in flight attitude input result in learning of values for roll, pitch and yaw tuning. In other words, airplane learns to fly based on external pilot behavior. Therefore, the pilot uses transmitter mode switch to switch to auto-tune mode and manual mode then flies the plane for a few minutes while it is "learning". By this reason, the auto-tune code can learn how the aircraft responds.
Furthermore, to begin with the experimentation to validate EKF and TECS algorithms, through auto-tune PID method, it is necessary to determine amount of tests and variables through experimental methods such as simple comparison method, one factor, variance analysis, random blocks, Latin squares or factorial design. To perform validation, experimental 2k method is then chosen, due to measurement of k factors along the process and its interaction; with this method, it can be obtained the desired information with the least amount of tests due to operational constraints [14]. For this process, 3 factors that could influence flight tests are chosen such as outside air temperature, pressure and wind speed vector. Flight test are performed in Bogota, located in the tropical high altitude plains of Colombian Andes. Test zone has coordinates 4.7110° N, 74.0721° W. It is located in a tropical zone where there are no seasons. Nevertheless, there is an eight-month rainy season with cloud presence and high wind speed [15]. Hence, using 2k method,

$$2^k = Number\ of\ tests \quad \textbf{(4)}$$

Equation 4 states that k is the number of variables. So, eight tests are performed to validate algorithms. Output parameters as attitude (pitch, roll, and yaw), height, airspeed, rate of climb and throttle are the matter of discussion of this article using a telemetry link (MavLink) and a dataflash log to record and send in real time data to a GCS (Ground Control Station). Finally, data such as stability derivatives and aircraft dynamic model is presented in order to determine transfer functions. Aerosim ® model is then used with Hardware in the Loop (HIL) simulation interface that replaces the plane and the environment with a simulator. Aerosim ® is very accurate with aircraft dynamics model and environment model (wind). Meanwhile, hardware is configured exactly for flight tests connected to GCS with the simulator, rather than the aircraft. This is to validate flight tests in order to determine percentage of error between real, theoretical and simulated data.

2. Experimental Arrangement

Physical properties of the Kadet Senior UAV system, its hardware and sensor setup are presented in this section. This is a first impress used to determine model dynamics to prepare flight experiments for the subsequent PID tuning and algorithms analysis. Two test platforms were used to obtain attitude and navigation data, Kadet K1 and Kadet K2, shown in figure 3. K1 is used to determine pitch, roll and yaw responses using manual mode to get initial data. K1 is a trainer model that uses an Ardupilot Mega APM 2.8 that includes 3-axis gyro, accelerometer with a high-performance barometer, external compass, onboard 4 MP dataflash chip for automatic datalogging, digital compass powered by Honeywell's HMC5883L-TR chip, a GPS uBlox NEO6, 6 DoF Accelerometer/Gyro MPU-6000 Atmel's ATMEGA2560 and ATMEGA32U-2 chips for processing. On the other hand, K2 UAV is equipped with 3D

DOI: 10.13009/EUCASS2017-411

Robotics Pixhawk autopilot, capable to perform both manual and automatic navigation using a GPS and an INS. The system has a brushless motor (1300wats) powered by two 6S LiPo batteries. Internal structure is able to carry a removable payload module that allows changing configuration depending on mission characteristics. Sensors can weigh as much as 800 grams to achieve a maximum endurance of 15 minutes at 2600 meters above sea level. Both airborne systems are integrated with the same GCS, which are composed by a radio transmitter to perform manual and automatic maneuvers. The operation management is performed by Mission Planner Software, which allows monitoring UAV data telemetry.

Kadet is manufactured by SIG Manufacturing Company, Inc., with electric propulsion powered by lithium polymer batteries. K1 and K2 are 1645 mm long with a 2045mm wing span, weigh 4950gr (without payload), and have 76.1 dm^2 of wing area with an average wing load of 65gr/dm^2. The power system consists of one brushless DC electric motor driving a 14 x 7 in propeller. The motor assembly turns the propeller up to 8500 RPM to develop about 1.4kg of thrust. Its airspeed ranges from a stall of 9 m/s to a maximum airspeed of about 35 m/s.

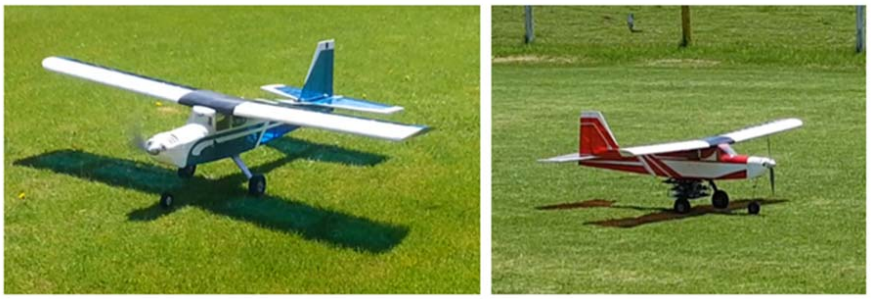

Figure 3: Test platforms K1 (Blue) and K2 (Red)

The Kadet K2 UAV has a conventional fixed-wing airframe, straight wing and high wing configuration with ailerons, rudder, and elevator control surfaces. In addition, control surfaces are actuated by Hitec® electric servos with a maximum deflection of 35deg in ailerons, 25deg in rudder and 20 deg in elevator. Properties of the airframe are shown in Table 1, the moments of inertia were calculated using XFLR5, as shown in figure 4 [16].

Table 1: KADET UAV physical properties

Property	Value	Unit
Mass (m)	4.95	kg
Wing Span (b)	2.045	m
Mean Aerodynamic chord ($\bar{c}$)	0.38	m
Wing area S	0.76	m^2
Moment of inertia Ixx	0.3175	$kg \cdot m^2$
Moment of inertia Iyy	0.3493	$kg \cdot m^2$
Moment of inertia Izz	0.5931	$kg \cdot m^2$
Moment of inertia Izz	0.002593	$kg \cdot m^2$

Consequently, aircraft is instrumented with a redundant IMU that measure angular rates and translational accelerations. Six gyroscopes form the angular rate sensor, and six accelerometers form the acceleration sensor. Pixhawh provides actuator commands at 30 Hz, IMU data is recorded at the 25Hz and telemetry link sends 3.56 data parameters per second. Flight tests are limited to line-of-sight due to Colombian aviation regulation. In addition, the pilot performs all takeoffs and landings, by this reason, all test are performed in cruise regime with 60% of throttle and 15m/s of desired airspeed.

DOI: 10.13009/EUCASS2017-411

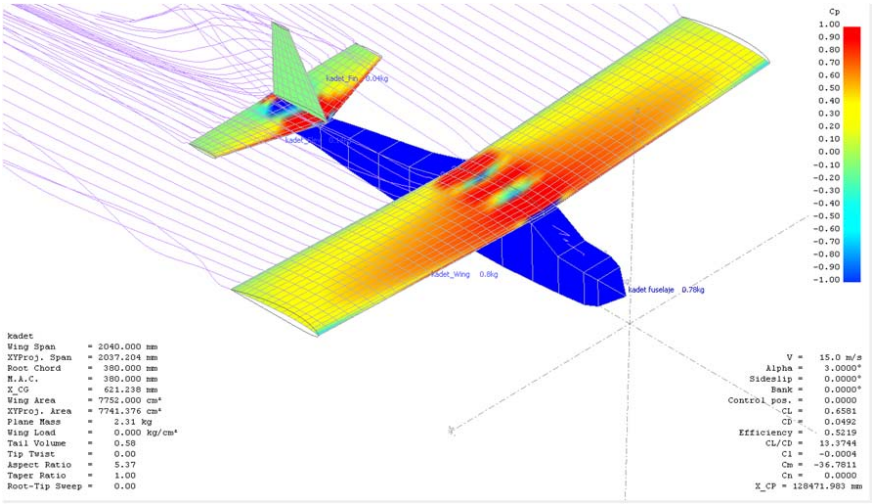

Figure 4: XFLR5 aerodynamic and stability analysis

3. Flight Experiment and Initial Tuning

In this section flight test planning and initial tuning methods are presented to create the conditions for the experimental validation. Typical flight experiments for UAV platforms are divided into three segments: takeoff, research experiments, and landing [17]. All conditions are described in cruise and small disturbances for climb, descent and coordinated turns to validate both EKF and TECS algorithms.

3.1 Flight Test

For this case, the study is focused on a typical flight dynamics test pattern [13], whereby the system or process corresponds to each of the flight stages to be evaluated, in order to enhance some analysis or simply to evaluate how far the actual behavior of the aircraft is compared to the predictions obtained from theoretical models. A diagram with the system is shown in Figure 5.

Figure 5: Factors involved during the experiment

When performing an experiment of an UAV in flight, there are uncontrollable factors (pressure, temperature and wind vector) that could drastically influence the error of the measurements and generate a high deviation of the output responses between each of the replicates of the experiment. For example, atmospheric conditions and unpredictable error of the experiments, as well as factors such as structural fatigue, aircraft maintenance, small variations due to engine vibrations and pilot technique, which will introduce variability in tests [18]. When uncontrollable factors of this type are found but can be measured, an analysis must be made to determine the error resulting from its influence.

DOI: 10.13009/EUCASS2017-411

According to Figure 5, prior to designing a flight plan that allows the aircraft dynamic information to be acquired correctly, it is essential to identify which parameters at the input of the system can be defined and which outputs are needed to analyze as a function of time. In addition, it is important to have clarity of the factors that can or cannot be controlled to know the possible sources of error that affect the output variables.

The object of study is to analyze the critical parameters of dynamics during the stages of cruise, climb and descent. Thus, variables that needed to be analyzed are identified; a flight plan focused on their measurement is generated in certain periods of time. The experiment airfield is first selected, which is described in Table 2.

Table 2: Experimental location parameters

Parameter	Value
Airfield location	Bogota, Colombia
Runway altitude	2570 m.a.s.l
Runway take off distance	300 m
Runway width	30 m
Latitude/Longitude	4,8240903 deg/ -74,1560519 deg
Runway heading	314º – 134º

During test flights, it was decided to acquire the information of the variables listed in Table 3, which are filtered after the flight and then analyzed to evaluate their variation with respect to the time and its interaction for each stage of flight.

Table 3: In Flight Measured parameters

Parameter	symbol	units
Time	t	s
Relative Altitude	h	m
Airspeed	V_a	m/s
Groundspeed	V_g	m/s
Wind Speed	V_w	m/s
Wind direction	B	deg
Vertical speed	V_v	m/s
Battery Remaining	B_R	%
Voltage Battery	V_B	V
Roll angle	ϕ	deg
Yaw angle	Ψ	deg
Pitch angle	Θ	deg
Roll rate	$\dot{\phi}$	deg/s
Yaw rate	$\dot{\Psi}$	deg/s
Pitch rate	$\dot{\Theta}$	deg/s
Throttle position	Tp	%
Elevator servo	PWM	ms

To generate flight plan, Mission Planner software is then used to program the desired route from latitude, longitude and altitude coordinates, along with some pre-established commands such as loiter, climb or descents to return to home. Figure 6 shows the proposed flight pattern which is intended to evaluate aircraft behavior during the climb, cruise and descent phases. It is proposed to develop several repetitions, at least 8, of the pattern for each phase at three different heights, in intervals of 100 meters and indirectly modify other non-controllable variables such as pressure, temperature and wind direction. KADET UAV takes off in manual mode until reaching an altitude of 100 m above the ground, and then automatic mode is switched to start the experiment.

DOI: 10.13009/EUCASS2017-411

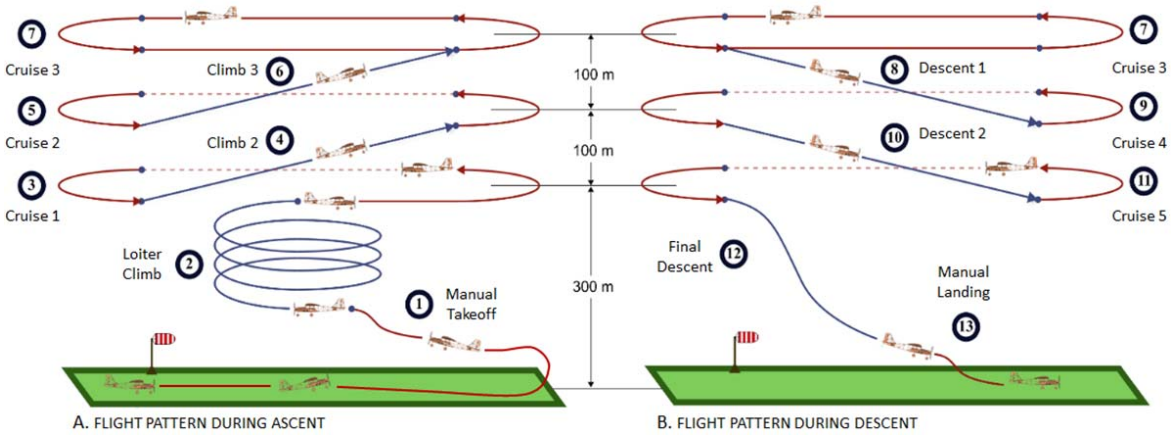

Figure 6: Experimental flight path

Experiment is performed in three paths that are defined at three different heights. Therefore, taking advantage of the variation of heights between each phase of cruise, it is proposed to evaluate three climbs and three descents for TECS algorithm. Also, it is defined to be evaluated through a spiral loiter with constant radius unlike the other two ascents that are made in a straight line for EKF algorithm. Similarly, for descent, the first two flight lines are set in straight trajectories and the last descent was conditioned to the command Return to Launch (RTL), which must take the aircraft back to 100m from a height of 300m to switch to manual mode for landing. On the other hand, runway selected for tests, usually presents winds in the direction 314deg of heading. For this reason, a standard heading for all heights was selected for the cruising stages, which is rectangular in shape with 500 meters in the direction of 314deg, to avoid the greatest number of cross-winds during the experiment, and paths of 350 meters perpendicular to the runway to evaluate the parameters under small disturbance conditions by lateral winds. The dimensions of the cruise pattern, climb and descent are detailed in Figure 7.

Last of all, tests are performed using trainer Kadet K1. Auto-tune mode is then used to setup the aircraft for initial PID values. Then, auto-tune level parameter from Ardupilot controller is defined; it controls how aggressive the tune will be. The default is level 6, which produces a medium tune, but it was selected level 7, which in faster attitude changes tuning. Basic settings are checked. In particular, all surface deflections and reversals and the minimum value of airspeed. Manual Radio control HiTec Aurora ® is calibrated because it only works for full control movements of pilot sticks. Manual tuning can result in better performance, but it takes more time and effort. Auto-tune mode tunes the P gain directly, but sets the D and I gain conservatively based on the auto-tune level, in this case 7, and value of the P gain. Figure 8 shows an example of 2 minutes session.

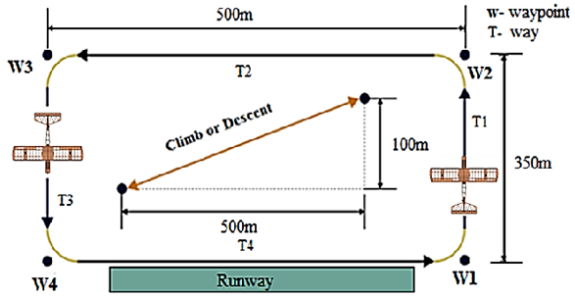

Figure 7: Top view cruise pattern

DOI: 10.13009/EUCASS2017-411

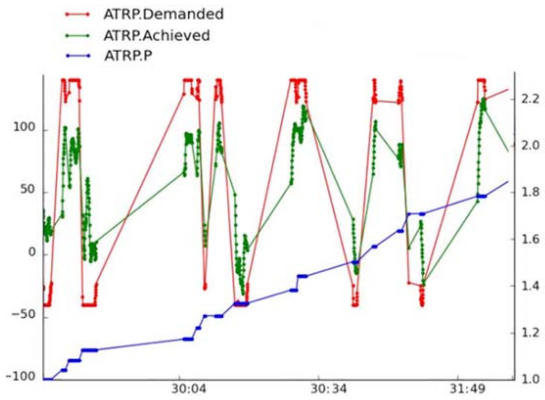

Figure 8: Kadet K1, Auto-tune session example

Auto-tune uses a message called ATRP; it has a type field that shows what type of auto-tune is being recorded. First type value is for roll tuning, and for pitch tuning. ATRP.P value is the P gain for the controller. ATRP.Achieved field is what the aircraft achieved in attitude change rate. ATRP.Demanded field is the demanded rate of attitude change (roll rate or pitch rate) in degrees per second. It can be seen in figure 8 that the tune progressed with the demanded and achieved started to converge [19]. Also, it is shown that the graph has some spaces; this is for periods where the pilot is not demanding a high rate of attitude change. D gains improve the accuracy of roll and pitch responses and makes the plane less affected by gusts and turbulence. The optimum value for D gain can be found by increasing the gain in small increments until the aircraft starts to oscillate. I gain reduces steady state error, and then this also changes the value for P that is required to maintain the correct response. A loop is generated until the airplane responded to the most efficient way.

4. Extended Kalman Filter EKF Analysis

In the following sections the general Extended Kalman Filter and three representative approaches for the attitude estimation problem are introduced, this methods are validated with experimental tests:

4.1 General extended Kalman filter

Assuming a general nonlinear discrete-time system where x_k is a $m \times 1$ vector, y_k is a $n \times 1$ vector, $f(x_{k-1}, u_k)$ and $g(x_k)$ are nonlinear functions. This system can be modeled as follows [20]:

$$x_k = f(x_{k-1}, u_k) + w_k \tag{5}$$

$$y_k = g(x_k) + v_k \tag{6}$$

The first equation is called the propagation equation and the second is called the measurement equation.

4.2 Quaternion based extended Kalman filter

This approach has many applications in state estimation problems and has been used by the UAV developers due to their simplicity. The system state variables are the unit quaternion (q) and the gyro biases (b_p, b_q, b_r). The measurements of the system are the three axes accelerations (a_x, a_y, a_z) and the yaw angle (Ψ) derived from the magnetometer [21] as shown in equations 7, 8 and 9.

DOI: 10.13009/EUCASS2017-411

$$\dot{q} = \frac{1}{2}\begin{bmatrix} 0 & -\hat{p} & -\hat{q} & -\hat{r} & 0 & 0 & 0 \\ \hat{p} & 0 & \hat{r} & -\hat{q} & 0 & 0 & 0 \\ \hat{q} & -\hat{r} & 0 & \hat{p} & 0 & 0 & 0 \\ \hat{r} & \hat{q} & -\hat{p} & 0 & 0 & 0 & 0 \\ \hline 0 & 0 & 0 & 0 & 0 & 0 & 0 \\ 0 & 0 & 0 & 0 & 0 & 0 & 0 \\ 0 & 0 & 0 & 0 & 0 & 0 & 0 \end{bmatrix} q + w_k \tag{7}$$

$$q = \begin{bmatrix} q_0 \\ q_1 \\ q_2 \\ q_3 \\ \hline b_p \\ b_q \\ b_r \end{bmatrix}, \begin{bmatrix} \hat{p} \\ \hat{q} \\ \hat{r} \end{bmatrix} = \begin{bmatrix} p \\ q \\ r \end{bmatrix} - \begin{bmatrix} b_p \\ b_q \\ b_r \end{bmatrix} \tag{8}$$

$$\begin{bmatrix} a_x \\ a_y \\ a_z \\ \Psi \end{bmatrix} = \begin{bmatrix} 2g(q_1q_3 - q_0q_2) \\ 2g(q_2q_3 + q_0q_1) \\ g(q_0^2 - q_1^2 - q_2^2 + q_3^2) \\ tan^{-1}\dfrac{2(q_1q_2 + q_3q_0)}{q_0^2 + q_1^2 - q_2^2 - q_3^2} \end{bmatrix} + v_k \tag{9}$$

4.3 Euler angle based extended Kalman filter

The attitude can be estimated using the follow equations where vector x is the system state (representig roll and pitch angle) and vector $\hat{y}$ is the system output (representing accelerometer readings).

$$x = \begin{bmatrix} \phi \\ \theta \end{bmatrix}, \ \hat{y} = \begin{bmatrix} a_x \\ a_y \\ a_z \end{bmatrix} \tag{10}$$

$$\dot{x} = \begin{bmatrix} p + qsin\phi tan\theta + rcos\phi tan\theta \\ qcos\phi - rsin\phi \end{bmatrix} + v_w \tag{11}$$

$$\hat{y} = \begin{bmatrix} \dot{u} - rv + qw - gsin\theta \\ \dot{v} + ru - pw - gcos\theta sin\phi \\ \dot{w} - qu + pv - gcos\theta cos\phi \end{bmatrix} + v_k \tag{12}$$

For small fixed-wing airplanes where are not easily measurable the three axes velocities (u, v, w) at high frequencies the air speed (V_a) can be used to simplify the measurement equation $(\hat{y})$. Some assumptions just be made like the small UAV will not accelerate all the time $(\dot{u} = \dot{v} = \dot{w} = 0)$, it does not have sideslip velocity $(v = 0)$, $u = V_a \cos\theta$ and $w = V_a \sin\theta$ [21]

$$\hat{y} = \begin{bmatrix} qV_asin\theta + gsin\theta \\ rV_acos\theta - pV_asin\theta - gcos\theta sin\phi \\ -qV_acos\theta - gcos\theta cos\phi \end{bmatrix} + v_k \tag{13}$$

The EKF algorithm implemented estimates a total of 18 states with the fundamental equations derived using the following process [4]:

Initial computation (algorithm):

1. Derivation of Navigation EKF using a local NED (North, East, Down) earth Tangent Frame
2. XYZ body fixed frame
3. Sequential fusion of velocity and position measurements
4. Fusion of true airspeed
5. Sequential fusion of magnetic flux measurements
6. Sequential fusion of angular LOS rate measurements from optical flow

DOI: 10.13009/EUCASS2017-411

7. Sensor assumed to be aligned with the Z body axis plus a small misalignment
8. 18 state architecture.
9. IMU data is assumed to arrive at a constant rate with a time step of dt
10. IMU delta angle and velocity data are used as time varying parameters

State vector:

1. Quaternions (q0, q1, q2, q3)
2. Velocity - m/sec (North, East, Down)
3. Position - m (North, East, Down)
4. Delta Angle bias - rad (X,Y,Z)
5. Delta Velocity bias - m/s (Z)
6. Wind Vector - m/sec (North,East)
7. Earth Magnetic Field Vector - milligauss (North, East, Down)
8. Body Magnetic Field Vector - milligauss (X,Y,Z)

Observations:

1. NED velocity - m/s
2. NED position - m
3. True airspeed - m/s
4. XYZ magnetic flux - milligauss
5. XY line of sight angular rate measurements from a downwards looking optical flow sensor range to terrain measurements

Time varying parameters:

1. XYZ delta angle measurements in body axes - rad
2. XYZ delta velocity measurements in body axes - m/sec

As it was shown in the algorithm, angular rates are integrated to calculate the angular position, accelerations are converted from X,Y,Z to earth NED axes and corrected for gravity, accelerations are integrated to calculate the velocity, velocity is integrated to calculate the position. Other states are taken into account as gyro biases, vertical acceleration, accelerometer bias, wind velocities, compass biases and the earth's magnetic field. Hence, gyro and accelerometer noise are used to estimate error in angles, velocities and position calculated. Error can be considerable high, if no corrections are made. These estimated errors are captured in a matrix called the State Covariance Matrix [4].The Extended Kalman Filter is able to use the correlation between different errors and different states to correct states other than the one being measured. GPS is able to correct errors in position, velocity, angles and gyro bias.

5. Total Energy Control System TECS

The objective of TECS design is to calculate the total energy state and desired state of an aircraft. Thrust controls the total energy error and elevator controls the energy distribution error. Therefore, it is important to derive the energy equations of an aircraft, especially for the total specific energy rate error and the specific energy rate distribution error [6]. Then, the aircraft distribution energy model can be derived from motion and energy equations.

5.1 Aircraft Energy Equations

The derivation of energy equations is based on Lambregts [23]. The total energy of an aircraft can be expressed as the sum of the potential energy and kinetic energy, as seen in equation3. Assuming constant weight, Equation 3 can be rewritten as:

$$E_T = mg\left(\frac{1}{2}\frac{V^2}{g} + h\right) \quad \textbf{(14)}$$

Using the small-disturbance theory, the energy of aircraft is linearized at steady flight conditions as:

$$E_{T0} + \Delta E_T = mg\left(\frac{1}{2}\frac{(V_0 + \Delta V)^2}{g} + (h_0 + \Delta h)\right) \quad \textbf{(15)}$$

Where V_0 is trimmed airspeed, it is assumed that$(\Delta V)^2 = 0$, Equation 18 with respect to time, yielding to:

DOI: 10.13009/EUCASS2017-411

$$\frac{d}{dt}(E_{T0} + \Delta E_T) = mg\frac{d}{dt}\left[\frac{1}{2}\left(\frac{V_0^2}{g} + \frac{2V_0\Delta V}{g}\right) + (h_0 + \Delta h)\right] \quad \textbf{(16)}$$

$$\Delta\dot{E} = mg\left(\frac{V_0\Delta\dot{V}}{g} + \Delta\dot{h}\right) \quad \textbf{(17)}$$

Dividing by the trimmed airspeed, V_0, yielding:

$$\frac{\Delta\dot{E}}{V_0} = mg\left(\frac{\Delta\dot{V}}{g} + \Delta\gamma\right) \quad \textbf{(18)}$$

Where γ is flight path angle (FPA). Hence, airspeed value and the rate of change of aircraft energy are dependent only upon the change of longitudinal acceleration, $\Delta\dot{V}$ and the change of flight path angle, $\Delta\gamma$ [23]. Propeller thrust helps to determine the total energy; this thrust can be derived from aircraft longitudinal equation of motion, as shown below:

$$m\Delta\dot{V} = \Delta T - \Delta D - mg\sin\Delta\gamma \quad \textbf{(19)}$$

Assuming that $\Delta\gamma$ is small, then $\sin\Delta\gamma = \Delta\gamma$, therefore

$$mg\left(\Delta\gamma + \frac{\Delta\dot{V}}{g}\right) = \Delta T - \Delta D \quad \textbf{(20)}$$

Thus, the aircraft rate of change of energy is proportional to the difference between thrust, T, and drag, D [6]. Rewriting the equation 23, the required thrust change as:

$$\Delta T = mg\left(\Delta\gamma + \frac{\Delta\dot{V}}{g}\right) + \Delta D = \frac{\Delta\dot{E}}{V_0} + \Delta D = \frac{\Delta\dot{E}_s}{V_0}mg + \Delta D \quad \textbf{(21)}$$

Where $\Delta\dot{E}_s$ is total specific energy rate. Assuming that the change of drag is negligible during the steady flight condition, the change of thrust is proportional to the sum of change of longitudinal acceleration and change of flight path angle [6]:

$$\Delta T \propto \left(\Delta\gamma + \frac{\Delta\dot{V}}{g}\right) \quad \textbf{(22)}$$

Thus, if the drag variation is slow, equations 21 and 24 show that the thrust required to maneuver is proportional to the specific energy rate of the system. Alternately, it can be stated that the throttle controls the rate at which energy can be added to or deleted from the system. In response to speed or flight path changes then, a control law can be developed that uses the throttles to drive the total energy rate error to zero [8] [24].

$$\delta_{T_C} = \left(K_{TP} + \frac{K_{TI}}{s}\right)\frac{\dot{E}_{S_E}}{V} \quad \textbf{(23)}$$

Where K_{TP} and K_{TI} are throttle proportional and integral gains respectively, δ_{T_C} is change in throttle command, $\dot{E}_{S_E}$ is total specific energy rate error and s is Laplace operator. Nevertheless, $\dot{E}_{S_E}/V$ is:

$$\frac{\dot{E}_{S_E}}{V} = \gamma_E + \frac{\dot{V}_E}{g} \quad \textbf{(24)}$$

This control law uses proportional plus integral control to reduce the total energy error to zero with a first order time constant, $\tau_E = K_{TP}/K_{TI}$ [23]. Correction of the energy rate distribution error can be accomplished by feeding back the difference of the acceleration error term $\dot{V}_E/g$ and the flight path angle error γ_E [24]. Using proportional plus integral control, the elevator control is:

$$\delta_{E_C} = \left(K_{EP} + \frac{K_{EI}}{s}\right)\left(\frac{\dot{V}_E}{g} - \gamma_E\right) \quad \textbf{(25)}$$

Where K_{EP} and K_{EI} are elevator proportional and integral gains respectively, δ_{E_C} is change in elevator command and $\dot{V}_E$ is rate of change of airspeed error.

DOI: 10.13009/EUCASS2017-411

Equations 26 and 28 form the TECS core algorithm, shows in figure 9, and are based on natural control behavior of the airplane and its control surfaces.

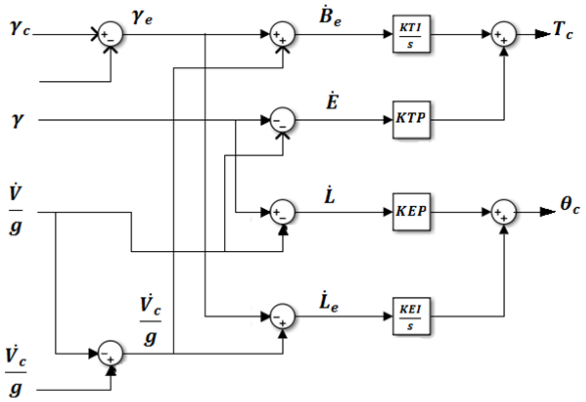

Figure 9: TECS core algorithm

7. Airplane Dynamic Model

In order to create the equations of movement it is required to consider the UAV as a rigid body. It is necessary to take into account the influence of mass and the moment of inertia. Also, aerodynamic damping effects are taken into account, but the effects of aeroelasticity are not considered. So, study of the dynamic stability, control and response of an aircraft implies the consideration of some assumptions established by Bryan, G. (1991) [25]. First, the instantaneous aerodynamic forces and moments depend only of instantaneous values of the motion variables in the three aircraft axes. Aerodynamic forces and moments vary linearly with the motion variables. Therefore, the equations are, in general, non-linear and are united in a single set; this is why an analytical solution is difficult. Therefore, it is assumed that the movement followed after a disturbance is characterized by small amplitudes in all disturbed variables. On the other hand, the aircraft has a vertical plane of symmetry and it is possible to linearize and separate the equations of motion into two groups, the first of which is longitudinal motion and the second, lateral directional motion.

For the formulation of the flight dynamics of an aircraft, it is necessary to consider different coordinate systems in such a way that the position, velocity, forces and moments acting on the aerial vehicle can be specified. The coordinate systems are as follows inertial axis system, fixed axle system to ground, navigation system and system of body axes [26].

$$x_{lon} = [u, w, q, \theta]^T \,, \quad \dot{x}_{lon} = A_{lon} x_{lon} + B_{lon} \delta_{elev} \tag{26}$$

First of all, longitudinal dynamics is decouple and analyzed taking into account the state equation
Where,

$$A_{lon} = \begin{bmatrix} X_u & X_w & X_q - W_e & -g\cos\theta_e \\ Z_u & Z_w & Z_q + U_e & -g\sin\theta_e \\ M_u & M_w & M_q & 0 \\ 0 & 0 & 1 & 0 \end{bmatrix}, \quad B_{lon} = \begin{bmatrix} X_{\delta_{elev}} \\ Z_{\delta_{elev}} \\ M_{\delta_{elev}} \\ 0 \end{bmatrix} \tag{27}$$

Matrixes represent state constants. We, Ue, and θe represent the trim condition. Finally, the linearized acceleration measurements are given by,

$$a_x = \dot{u} + qW_e + g\cos\theta_e\theta + g\sin\theta_e \,, a_z = \dot{w} - qU_e + g\sin\theta_e\theta - g\cos\theta_e \tag{28}$$

Likewise, lateral directional is couple between roll and yaw conditions, so the state equation and acceleration is given by,

$$\boldsymbol{x_{lat}} = [\boldsymbol{v}, \boldsymbol{p}, \boldsymbol{r}, \boldsymbol{\phi}, \boldsymbol{\psi}]^T \,, \quad \boldsymbol{M_{lat}\dot{x}_{lat}} = \boldsymbol{A'_{lat}x_{lat}} + \boldsymbol{B'_{lat}}\begin{bmatrix} \boldsymbol{\delta_{ail}} \\ \boldsymbol{\delta_{rud}} \end{bmatrix} \tag{29}$$

DOI: 10.13009/EUCASS2017-411

$$M_{lat} = \begin{bmatrix} 1 & 0 & 0 & 0 & 0 \\ 0 & 1 & -I_{xz}/I_x & 0 & 0 \\ 0 & -I_{xz}/I_z & 1 & 0 & 0 \\ 0 & 0 & 0 & 1 & 0 \\ 0 & 0 & 0 & 0 & 1 \end{bmatrix} A'_{lat} = \begin{bmatrix} Y_v & Y_p + W_e & Y_r - U_e & g\cos\theta_e & 0 \\ L_v & L_p & L_r & 0 & 0 \\ N_v & N_p & N_r & 0 & 0 \\ 0 & 1 & \tan\theta_e & 0 & 0 \\ 0 & 0 & \sec\theta_e & 0 & 0 \end{bmatrix} \quad \textbf{(30)}$$

$$B'_{lat} = \begin{bmatrix} Y_{\delta_{ail}} & Y_{\delta_{rud}} \\ L_{\delta_{ail}} & L_{\delta_{rud}} \\ N_{\delta_{ail}} & N_{\delta_{rud}} \\ 0 & 0 \\ 0 & 0 \end{bmatrix}$$

$$a_y = \dot{v} - pW_e + rU_e - g\cos\theta_e\emptyset \quad \textbf{(31)}$$

Longitudinal and lateral-directional control and stability derivatives, velocity, and equilibrium terms are estimated using XFLR5 data. The angular rate stability derivatives are taken from values estimated in flight for KADET. Along with mass data from Table 1, the longitudinal and lateral-directional model baseline model is given by,

$$A_{lon} = \begin{bmatrix} -0.43 & 0.65 & -0.38 & -7.80 \\ -0.48 & -6.81 & 13.32 & -0.11 \\ 0.19 & -7.24 & -37.23 & 0 \\ 0 & 0 & 1 & 0 \end{bmatrix}, B_{lon} = \begin{bmatrix} -0.43 \\ -3.13 \\ -96.32 \\ 0 \end{bmatrix}, M_{lat} = \begin{bmatrix} 1 & 0 & 0 & 0 & 0 \\ 0 & 1 & -0.143 & 0 & 0 \\ 0 & -0.001 & 1 & 0 & 0 \\ 0 & 0 & 0 & 1 & 0 \\ 0 & 0 & 0 & 0 & 1 \end{bmatrix} \quad \textbf{(32)}$$

$$A'_{lat} = \begin{bmatrix} -1.35 & 0.63 & -17.5 & 7.85 & 0 \\ -1.13 & -11.41 & 23.71 & 0 & 0 \\ 0.33 & -0.13 & -6.14 & 0 & 0 \\ 0 & 1 & 0.001 & 0 & 0 \\ 0 & 0 & 1 & 0 & 0 \end{bmatrix}, B'_{lat} = \begin{bmatrix} 0 & 5.2 \\ -45.1 & 17.3 \\ -7.01 & -16.5 \\ 0 & 0 \\ 0 & 0 \end{bmatrix} \quad \textbf{(33)}$$

Longitudinal and lateral-directional dynamics are computed from an eigenvalue of the system state matrix and presented in Table 4.

Table 4: Starting point longitudinal lateral-directional dynamics

Mode	Natural frequency, rad/s	Damping ratio
Phugoid	0.33	0.63
Short-period pole 1	11.5	-- --
Spiral	0.01	-- --
Dutch roll	5.1	0.43
Roll	11.5	-- --

8. Telemetry analysis and results

In this section is presented the results that validate theory of TECS and EKF algorithm through flight tests. It is shown the most important parameters taken into account in the analysis. An 80 seconds flight path was selected for presentation purposes during different stages of profile mission. Figure 10 shows TECS validation using airspeed, throttle position, pitch angle and relative altitude. TECS algorithm, showed a 12.3% Pitch, 5.5% airspeed of error and 11.1 % relative altitude with the real world model, it can be inferred that Algorithm is very accurate, some variables needed to be taken into account to reducer disturbances errors.

On the other side, EKF algorithm is validated using equations of motion and system state variables. It was very difficult to make a real estimation due to changes of angular positions and rates due to wind and turbulence, disturbances, taken into account and filtered by data extractions.

DOI: 10.13009/EUCASS2017-411

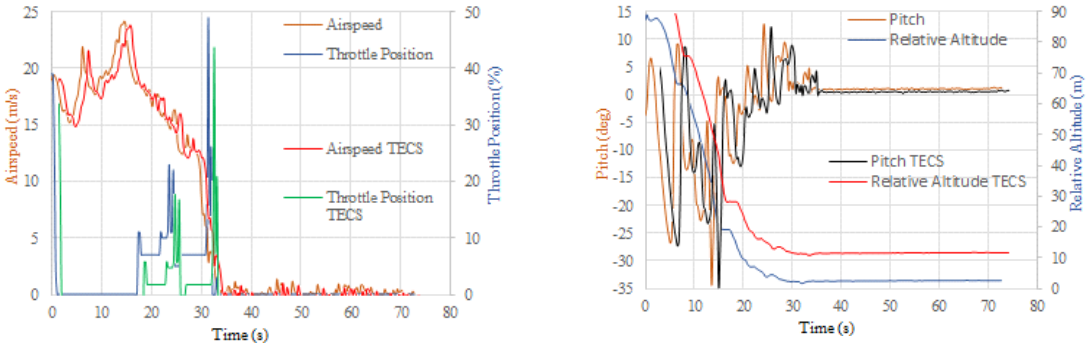

Figure 10: TECS Validation

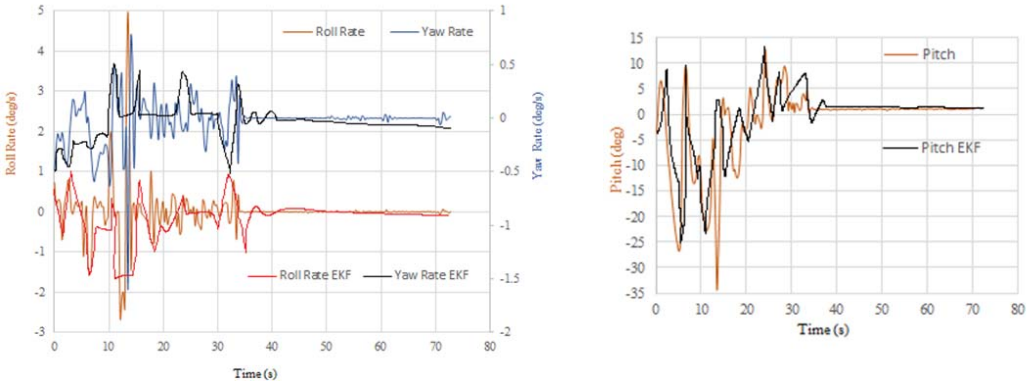

Figure 11: EKF Validation

Figure 11 shows that the models precisely predict the aircraft response, and, that the EKF algorithm matches closely, it is found an error of 9.5% on average. The elevator response confirms that the longitudinal and lateral- directional dynamics are decoupled. The yaw rate response shows discrepancy from the models, this due to the use of L1 controller for navigation between waypoints [12] that are out of range of this research.

Conclusions

A validation using flight tests and theoretical approaches of TECS and EKF algorithms was developed to accurately model the dynamics and control of fixed-wing UAV. Aircraft dynamics and control are analyzed in the time domain by adjusting nonlinear models to estimate time responses. On the other hand, it is evident that longitudinal stability increases if the center of gravity is in a forward position, within the allowed ranges. Due to disturbances by wind gusts during the experiment, it was difficult for the aircraft to fly straight and level, which influences the results, because at most instants of time it had major or minor angles of attack and did not maintain the 2 degrees of incidence. Due to air disturbances, the aircraft could not maintain constant height during cruise, but due to the corrections of the elevator it is kept oscillating within a range of heights of 4 meters. Because the aircraft took a long time to stabilize during turns, it is recommended to increase the length of the flight pattern for a more effective sampling. The main advantage of the proposed approach is the successful validation of aircraft dynamics and control using flight data from a single, low-cost inertial sensor. A drawback to the approach is that the analysis cannot be performed in real time different frequency samples from sensors were corrected in order to compare data at the same frequency. In summary, the procedure was defined to obtain models that are useful in control applications for aircraft equipped with low-cost sensors, for future uses.

Acknowledgments

This project is the result of a research process supported by Universidad de San Buenaventura Bogota, Colombia. Everything was possible thanks to the research work prepared by students, professors and graduates in Aeronautical

DOI: 10.13009/EUCASS2017-411

Engineering faculty, who made everything possible through all previous studies who involved the development of Unmanned Vehicles. We thank University of San Buenaventura, who provided the related laboratories and economic support to develop the project. We would also like to show our gratitude with the students Luz Angela Ibarra and Ramiro Zuluaga for helped us in the development and adjustment of RC airplanes who made this research possible.

References

[1] Eure, K., Quach, C., Vazquez, S., Hogge, E., and B. Hill. 2013. An Application of UAV Attitude Estimation Using a Low Cost Inertial Navigation System. Paper. Langley.

[2] Huang, S. 2010. Understanding Extended Kalman Filter. Paper. Sydney.

[3] Chao, H., Coopmans, C., Di, L., and Y. Chen. 2010. A Comparative Evaluation of Low-Cost IMUs for Unmanned Autonomous Systems. Paper. Salt Lake.

[4] ArduPilot Dev Team. 2016. Extended Kalman Filter Navigation Overview and Tuning. [Online]. Available: http://ardupilot.org/dev/docs/extended-kalman-filter.html.

[5] Qiping, C., Mulder, B., Choukroun, D., Kampen, E.-J., Visser, C., and G. Looye. 2013. *ADVANCES IN. Aerospace Guidance, Navigantion and Control*. Paper. Springer, Berlin, Heidelberg.

[6] Lambregts, A. A. 1983. Vertical Flight Path and Speed Control Autopilot Design Using Total Energy Principles. American Institute of Aeronautics and Astronautics, Vols.1, AIAA 1983-2239. Paper.

[7] Lambregts, A. A. 1984. Total energy based flight control system. Patent WO1984001345 A1.

[8] Faleiro, L.F., Lambregts, A.A. 1999. Analysis and tuning of a 'Total Energy Control System' control law using eigenstructure assignment. AerospaceScience and Technology, No. 3. Paper. Oberpfaffenhofen.

[9] Kelly, J., Person, L., and Bruce, K. 1986. Flight Testing TECS — The Total Energy Control System. SAE International. Paper.

[10] Brigido-González, J. D., and Rodríguez-Cortés, H. 2016. Experimental Validation of an Adaptive Total Energy Control System Strategy for the Longitudinal Dynamics of a Fixed-Wing Aircraft. Journal of Aerospace Engineering, Volume 29. Paper.

[11] Robert Balmer, G. 2015. Modelling and Control of a Fixed-wing UAV for Landings on Mobile Landing Platforms. Paper. Stockholm.

[12] ArduPilot Dev Team. 2016. TECS (Total Energy Control System) for Speed and Height Tuning Guide. [Online]. Available: http://ardupilot.org/plane/docs/tecs-total-energy-control-system-for-speed-height-tuning-guide.html

[13] Jiménez, P., Rafael C., Eliana, Z., and Daniel, A. 2017. Diseño, análisis y validación de aeronaves no tripuladas multipropósito. Libro resultado de investigación.

[14] Ferré, J. 2005. El diseño factorial completo 2k. [Online]. Available: http://rodi.urv.es/quimio/general/doecast.pdf

[15] Jiménez, P., Daniel, A. 2015. Validation and Calibration of a High-Resolution Sensor in Unmanned Aerial Vehicles for Producing Images in the IR Range Utilizable in Precision Agriculture. Capítulo de Libro, p. 15-23.

[16] XFLR5 Dev Team. 2017. XFLR5 Software.

[17] Dorobantu, A., Murch, A., Mettler, B., and G. Balas. 2013. System Identification for Small, Low-Cost, Fixed-Wing Unmanned Aircraft. Paper. Journal of Aircraft, Vol. 50, No.4.

[18] Tucker, A. 2012. Safety, Efficacy, and Efficiency: Design of Experiments in Flight Test. Anaheim, California: Society of Experimental Test Pilot, Annual Symposium 56th, pp. 2-10.

[19] ArduPilot Dev Team. 2016. Automatic Tuning with AUTOTUNE. [Online]. Available: http://ardupilot.org/plane/docs/automatic-tuning-with-autotune.html

[20] Welch, G., and Bishop, G. 2006. An Introduction to the Kalman Filter. University of North Carolina at Chapel Hill. [Online]. Available: https://www.cs.unc.edu/~welch/media/pdf/kalman_intro.pdf

[21] Jang, J. S., and Liccardo, D. 2007. Small UAV automation using MEMS. IEEE Aerospace and Electronic Systems Magazine, Vol. 22, No. 5, pp.30–34.

[22] Beard, R., Kingston, D., Quigley, M., Snyder, D., Christiansen, R., Johnson, W., McLain, T., and Goodrich, M. 2005. Autonomous vehicle technologies for small fixed wing UAVs. Journal of Aerospace Computing, Information, and Communication, Vol. 5, No. 1, pp. 92–108.

[23] Lai, Y. C., and Ting, W. 2016. Design and Implementation of an Optimal Energy Control System for Fixed-Wing Unmanned Aerial Vehicles. Article. Journals Applied Sciences.

[24] Bruce, K. R. 1987. NASA B737 Flight Test Results of the Total Energy Control System. Report No. NASA CR-178285.

[25] Bryan, G. and Hartley, G. 1911. Stability in aviation; an introduction to dynamical stability as applied to the motions of aeroplanes. London, Macmillan and Co., limited.

[26] Pamadi, B. N. 2004. Performance, Stability, Dynamics, and Control of Airplanes. American Institute of Aeronautics and Astronautics, Cap. 5.